Journal of the European Ceramic Society 38 (2018) 1508–1516

Contents lists available at ScienceDirect

Journal of the European Ceramic Society

journal homepage: www.elsevier.com/locate/jeurceramsoc

Original Article

Phase composition, crystal structure and microwave dielectric properties of $Mg_{2-x}Cu_xSiO_4$ ceramics

Yuanming Lai[a], Xiaoli Tang[a], Xin Huang[a], Huaiwu Zhang[a], Xiaofeng Liang[b], Jie Li[a], Hua Su[a,*]

[a] State Key Laboratory of Electronic Thin Films and Integrated Devices, University of Electronic Science and Technology of China, Chengdu 610054, PR China
[b] Analytical and Testing Center, Southwest University of Science and Technology, Mianyang 621010, PR China

ARTICLE INFO

Keywords:
$Mg_{2-x}Cu_xSiO_4$ ceramics
Phase composition
Crystal structure
Microwave dielectric properties

ABSTRACT

In this work, the $Mg_{2-x}Cu_xSiO_4$(x = 0–0.40) microwave dielectric ceramics were prepared using solid-state reaction method. Compared with the Mg_2SiO_4 sample, the Cu-substituted Mg samples could be sintered at a lower temperature. The $Mg_{2-x}Cu_xSiO_4$ ceramics exhibit the composite phases of Mg_2SiO_4 and a small quantity of $MgSiO_3$. The Cu^{2+} ion presented a solid solution with the Mg_2SiO_4 phase and preferentially occupy Mg(1) site. The distortion of MgO_6 octahedron was modified by Cu^{2+} ions, resulting in a positive change in the temperature coefficient of resonance frequency (τ_f) values. Excellent microwave dielectric properties of ε_r = 6.35, high Qf of ~ 188,500 GHz and near zero τ_f = −2.0 ppm/°C were achieved at x = 0.08 under sintering at 1250 °C for 4 h. Thus, the fabricated ceramics were considered as possible candidates for millimeter-wave device applications.

1. Introduction

Dielectric materials have recently garnered considerable attention owing to their practical applications in microwave telecommunication. In practical applications, the important characteristics required for concerning material used in microwave telecommunication are as follows. (a) the dielectric constant should be low so as to shorten the delay time of signal, whereas the Qf should be as high as possible; and (b) the microwave ceramics must simultaneously require a near-zero temperature coefficient of resonance frequency (τ_f) and a similarly low sintering temperature.

Mg_2SiO_4 ceramics has been extensively researched because of its low dielectric constant (ε_r = 6–7) and high Qf value (~240,000 GHz). However, pure Mg_2SiO_4 ceramics possess largely negative temperature coefficients of resonance frequency (τ_f = −67 ppm/°C) and require high sintering temperature (1350–1450 °C), directly limiting its practical use [1–3]. In order to develop the τ_f value to near-zero, TiO_2 (τ_f ~ +450 ppm/°C) and $CaTiO_3$ (τ_f ~ +850 ppm/°C) were added [3–5]. In addition, several methods were conducted to reduce sintering temperature, including addition of low melting oxides or glass [6–9]. However, these additives can lead to the deterioration of microwave dielectric properties or significantly increase the possibility of chemical interaction with the metal electrode because of the appearance of unexpected secondary phases.

In general, the dielectric loss and temperature stability of these ceramics are closely related to crystal structure. Cation ordering and tilting of the oxygen octahedra are the main structural features that affect the microwave dielectric properties of these materials [10]. Earlier reports showed that τ_f would depend on the average octahedral distortion in Mg-based ceramics [11]. Mg_2SiO_4 crystal, which is an orthorhombic structure that belongs to the Pbnm space group, consists of isolated SiO_4 tetrahedra surrounded by MgO_6 octahedra occupying sites of two different symmetries ($Mg(1)O_6$ and $Mg(2)O_6$). The $Mg(1)O_6$ site is slightly smaller and flattened along its threefold axis. The $Mg(2)O_6$ site is slightly larger and considerably more distorted. Given that Si^{4+} is nearly invariably stoichiometric, compositional variations occur in the two octahedral sites. Thus, adjustment of the τ_f values can be effectively achieved by changing the MgO_6 average octahedral distortion. Substitution of a cation with lower ionic radii for the ion with larger ionic radii improved the microwave dielectric properties. To improve the microwave dielectric properties of Mg_2SiO_4 ceramics by various ionic substitution, such as divalent cations Ni^{2+}, Mn^{2+}, Ca^{2+} and Zn^{2+} ions and tetravalent Ti^{4+} ions are substituted for Mg^{2+} and Si^{4+} ions, respectively [1,12–15]. However, these materials demand high densification temperature. CuO has been widely used as sintering aid of microwave dielectric ceramic because of its low melting point (1086 °C). Recently, CuO as sintering aid were added to the $BaSm_2Ti_4O_{12}$ and $Mg(Zr_{0.05}Ti_{0.95})O_3$ ceramics to decrease the sintering temperature [16,17]. In addition, the similar ionic radius between Cu^{2+} (0.73 Å) and Mg^{2+} (0.72 Å) ions can facilitate the easy entry of

* Corresponding author.
E-mail address: uestcsh77@yahoo.com (H. Su).

http://dx.doi.org/10.1016/j.jeurceramsoc.2017.10.035
Received 15 August 2017; Received in revised form 17 October 2017; Accepted 18 October 2017
Available online 19 October 2017

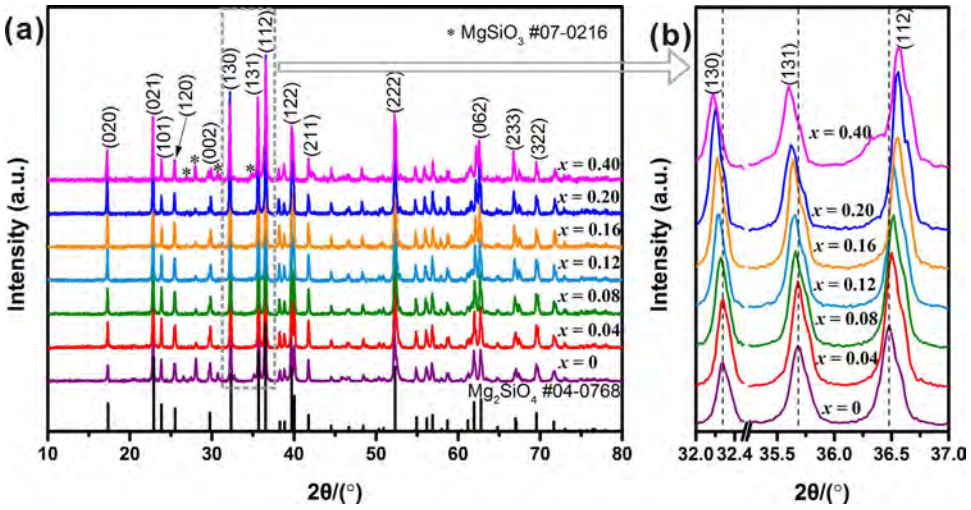

Fig 1. XRD of the $Mg_{2-x}Cu_xSiO_4$ (x = 0–0.40) ceramics sintered at 1250 °C (a) and the 2 θ range 32–37° (b).

Cu^{2+} ions into Mg sites and change the MgO_6 average octahedral distortion.

In the present work, given the low melting temperature (~1026 °C) of CuO and the similar ionic radii of Cu^{2+} (0.73 Å) and Mg^{2+} (0.72 Å), the investigation of lower sintering temperature and the possible improvement of microwave dielectric properties in Mg_2SiO_4 ceramics by Cu substitution for Mg is of considerable interest. $Mg_{2-x}Cu_xSiO_4$ (x = 0–0.40) ceramics were prepared through the solid-state ceramic route. XRD, XRD refinement, SEM, Raman spectra and microwave dielectric properties were carried out to assess the correlation among compositions, structure and properties.

2. Experimental procedure

$Mg_{2-x}Cu_xSiO_4$ ceramics were prepared via the solid-state ceramic route. Analytically pure MgO, CuO and SiO_2 (Sinopharm Chemical Reagent Co., Ltd) were used as starting materials; the materials were weighed and wet mixed in distilled water by using zirconia balls in a plastic container for 4 h. The slurry was dried and calcined in alumina crucibles at 1200 °C for 4 h. The calcined powders were well ground into a fine form and pressed under a uniaxial pressure of 10 MPa into cylindrical disks with 12 mm diameter and 4–5 mm height. Sintering was carried out at temperature levels between 1100 °C–1350 °C for 4 h.

The crystalline phase of the ceramics was confirmed using PANalytical X'Pert PRO with Cu K_α radiation (λ = 1.54 Å) at room temperature. The XRD patterns were measured in the 2θ angle range between 10° and 120° with a step of 0.02° and a time per step of 1.0 s. The structure refinements were conducted using Rietveld's method, for which FullProf software was used. The microstructures and morphology of the sintered samples were analysed by a scanning electron microscope (SEM) (JSM-6490; JEOL, Japan) at an accelerating voltage of 20 kV. The Raman spectra were obtained using an InVia Raman microscope (Renishaw, UK) with an argon ion laser (λ = 514.5 nm) as the excitation light. Raman shifts are measured with a precision of ~0.3 cm^{-1}. The spectral resolution is of the 1 cm^{-1} order. The spectra were recorded in the range of 150–1200 cm^{-1}. The density of each sample was measured at room temperature by Archimedes method with distilled water as the buoyancy liquid. Microwave dielectric properties were measured with a Vector Network Analyzer (N5230, Agilent Technologies, USA). The relative dielectric constants (ε_r), quality factor (Qf) and temperature coefficient of resonance frequency (τ_f) of the samples were determined, respectively, by the Hakki-Coleman dielectric resonator method and cavity methods in the frequency range 10–16 GHz with a TE011 resonant peak.

The site preference of Cu atoms in $Mg_{2-x}Cu_xSiO_4$ was investigated by density functional theory. The first-principle calculations within the framework were performed using the CASTEP software package implemented in Materials Studio software. The calculations of the local density approximation (LDA) functional with plane–wave basis sets and pseudopotential approximation were conducted to describe the total energy of the $Mg_{1.92}Cu_{0.08}SiO_4$ considered in this study. For ensuring the convergence of the ground-state total energy, the cut-off energy of the plane–wave basis was set to 990 eV and the 5 × 2 × 4 Monkhurst–Pack k-mesh was adopted. We set the convergence tolerance to 5.0×10^{-6} eV/atom. For geometric optimisation, both cell parameters and internal atomic coordinates were relaxed by using a force tolerance of 0.01 eV/nm. The total energies of Cu^{2+} ions preferring the Mg(1) and Mg(2) sites were obtained through calculations.

3. Results and discussion

The XRD patterns of the $Mg_{2-x}Cu_xSiO_4$ ceramics sintered at 1250 °C are shown in Fig. 1(a). Notably, the main phase were the Mg_2SiO_4 (ICDD No.#04-0768) with increasing x. The secondary phase, $MgSiO_3$ (ICDD No.#07-0216), was also detected, whereas the containing-Cu phases were not detected in all samples. These outcomes indicate that Cu^{2+} ions could enter into the lattice of the Mg_2SiO_4 phase. In addition, the diffraction peaks of (130) and (131) lattice planes tend toward lower diffraction angles; whereas (112) lattice planes tend toward higher diffraction angles (Fig. 1(b)). This trend indicates that cell parameters can vary because of Cu-substituted Mg. Moreover, for $0.04 \le x \le 0.20$, the XRD patterns of $MgSiO_3$ weakened significantly compared with the x = 0 and 0.40, indicating that moderate CuO can suppress the secondary phase ($MgSiO_3$). The reaction can be expressed as follows:

$$MgSiO_3 + CuO \leftrightarrow MgCuSiO_4 \quad (1)$$

For studying the details of the crystal structures with Cu-substituted Mg, the whole XRD pattern was refined using the Fullprof program [18]. Such refinement involved within the orthorhombic structural models of Mg_2SiO_4 (a = 4.7600 Å, b = 10.2000 Å and c = 5.9900 Å) and $MgSiO_3$ (a = 18.2110 Å, b = 8.8100 Å and c = 5.2030 Å) with the space groups Pbnm and Pbca, respectively. The crystal structure of

Table 1
Total energies and band gaps for pure-Mg_2SiO_4 and $Mg_{1.92}Cu_{0.08}SiO_4$ with Cu atoms placed at the Mg(1) sites and Mg(2) sites, respectively.

Cu occupying site	Total energy (eV)	Band gap (eV)
Non-Cu	−20113.771	4.85
Mg(1)	−19355.597	3.77
Mg(2)	−18972.538	3.12

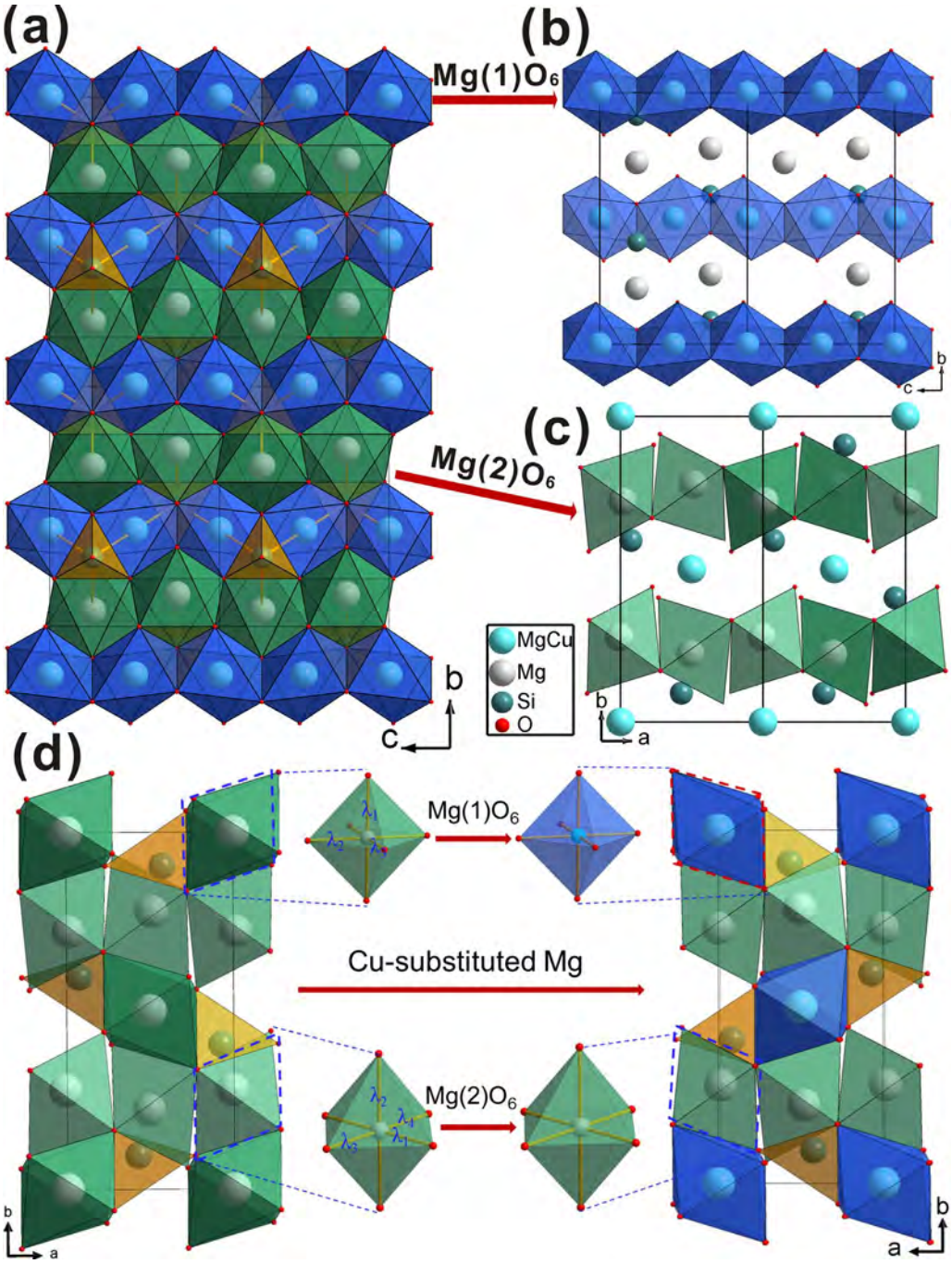

Fig. 2. (a) The crystal structure patterns of the (2 × 2 × 2) supercell of the $Mg_{1.92}Cu_{0.08}SiO_4$. (b) $Mg(1)O_6$ octahedral unit. (c) $Mg(2)O_6$ octahedral unit. (d) The schematic of substituted Cu for Mg in $Mg_{2-x}Cu_xSiO_4$ (left: $x = 0$, right: $x = 0.08$).

forsterite is composed of SiO_4 tetrahedra, $Mg(1)O_6$ and $Mg(2)O_6$ octahedra. Previous studies found that the Mg(1) site is flattened along its threefold axis, yet the Mg(2) site is notably more distorted [19]. This finding means that cations with relatively high octahedral site preference energies are more electronegative; for example, Ni^{2+} and Co^{2+} ions exhibit preference for the Mg(1) site [12,13,19,20]. In addition, the total energy was obtained by first-principle calculation (Table 1). Compared with pure Mg_2SiO_4, the substituted ceramics present higher total energy, which indicates that structural stability deteriorates with the substitution of Mg^{2+} ions by Cu^{2+} ions. However, Cu^{2+} ions substituted in the Mg(1) site yields a markedly lower total energy compared with the Mg(2) site, the energy difference being 383.059 eV. Thus, the total energy-minimised structures indicate a strong preference for Cu^{2+} ions to occupy the Mg(1) site. The DOS shows a band gap of 3.77 eV for $Mg_{1.92}Cu_{0.08}SiO_4$, with Cu^{2+} occupying the Mg(1) site compared with a band gap of 3.12 eV with Cu^{2+} occupying Mg(2) site. Larger band gap indicates higher stability in terms of lowering the band energy [21]. In general, mere size consideration would imply that Cu^{2+} ions preferentially occupy Mg(2) site because the ionic radius of Cu^{2+} (0.73 Å) is larger than that of Mg^{2+} (0.72 Å). However, the minimum total-energy was obtained when Cu^{2+} ions occupy the Mg(1) site. The lowering of energy levels can occur through increased covalence effect between metal *d* and *p* levels of the neighbouring oxygen sites [21]. In addition, the neighbouring $Mg(1)O_6$ octahedral units share the oxygen edges of neighbouring octahedra to form chains, while $Mg(2)O_6$ octahedral units form a network by sharing oxygen atoms from neighbouring octahedra with reduced connectivity (Fig. 2 (b) and (c)). This causes enhanced covalency in case of Mg(1) occupied situation which is found to be sufficient enough to overcome the size preferred Mg(2) occupied situation [21]. Thus, the occupancy of Cu^{2+} should be

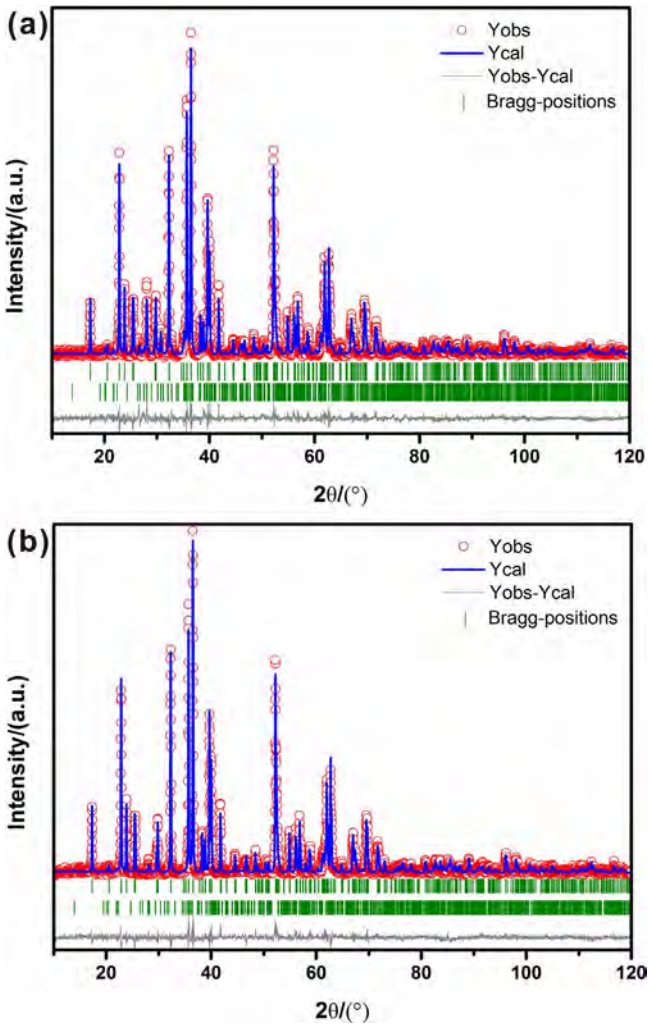

Fig. 3. Rietveld refinements of XRD pattern for $Mg_{2-x}Cu_xSiO_4$ sintered at 1250 °C, (a) $x = 0$, (b) $x = 0.08$, showing the experimental and the calculated profile.

assigned to the Mg(1) site of forsterite in the refinement. As representative data, the refined XRD patterns of the $x = 0$ and 0.08 ceramics are shown in Fig. 3 and *Table S1 (Supplementary information)*. All fitted curves match well with the experimental data, and the positions of the Bragg reflections are consistent with the indexed peaks. In addition, the reliability factors of refinement and the percentages of the phases are presented in Table 2. The schematic diagram of Cu-substituted Mg(1) is depicted in Fig. 2(d).

As observed from the refinement results, the lattice constant *b* values increase with the increase in *x* values, while the *a* values are almost constant and c values decrease (Fig. 4). This finding is consistent with the shift of diffraction peaks (Fig. 1(b)). A nearly linear dependence can be observed between the lattice parameters and *x* value, which is consistent with Vegard's law and also confirms the formation of a solid solution. Moreover, unit cell volumes first increase and then slightly decrease as $x = 0.40$ (Fig. 4). The larger value of unit cell volumes for Cu^{2+} substitution could be due to the larger size of the substituted Cu^{2+} ions ($r = 0.73$ Å) compared with that of Mg^{2+} ($r = 0.72$ Å) ions.

In addition, the atomic interactions of Mg_2SiO_4 ceramics can be modified because of the substitution of Mg^{2+} ions by Cu^{2+} ions, which could result in a change in the bond length of the MgO_6 octahedron. The variations of the cation–oxygen bond length are presented in *Table S2 (Supplementary information)*. The cation–oxygen bond lengths present different trends with the substitution of Mg^{2+} ions by Cu^{2+} ions. Bond lengths of Mg(1)–O(3) increase, whereas those of Mg(2)–O(3)^2 decrease with substitution of Mg^{2+} ions by Cu^{2+} ions. The findings imply that the MgO_6 octahedra are distorted according to the definition as follws [11,22,23]:

$$\delta = \frac{1}{6}\Sigma\left(\frac{R_i - \bar{R}}{\bar{R}}\right)^2 \quad (2)$$

where R_i is the individual bond length, and $\bar{R}$ is the average bond length of the MgO_6 octahedron. Given the Rietveld refinement of the XRD and Eq. (2), the MgO_6 octahedral distortions are listed in *Table S3 (Supplementary information)*. The distortion of the $Mg(1)O_6$ octahedron is less than those of the $Mg(2)O_6$ octahedron, which is in accordance with the structural characteristics of Mg_2SiO_4. The distortions of octahedron present nonlinear variation with the substitution of Mg^{2+} ions by Cu^{2+} ions, which is an intrinsic factor found to affect microwave dielectric properties [24].

The SEM images of the $Mg_{2-x}Cu_xSiO_4$ ceramics sintered at different temperatures are shown Fig. 5. As shown, the grain size increase with increasing Cu^{2+} ion content sintered at 1250 °C. As $x \leq 0.08$, a small amount of pores with smaller grains size of 0.5 ~ 3 μm were observed. As $0.12 \leq x \leq 0.16$, homogeneous distribution of grains size and densification was obtained, whereas the grain boundary disappeared as excess Cu-substituted Mg because of the appearance of liquid phase (Fig. 5 (e)). This indicated that a moderate amount of Cu substitution could significantly improve the densification behavior of the Mg_2SiO_4 ceramics. Compared the different sintered temperature as $x = 0.08$ and 0.12, the low sintered temperature exhibited a small amount of pores with smaller grains size (Fig. 5(f) and (i)). High sintered temperature presented a relatively dense microstructure. But the distribution of grains size showed heterogeneity (Fig. 5(g), (h) and (j)). The dense and uniform microstructure was achieved in the sample with $0.12 \leq x \leq 0.16$ sintered at 1250 °C, which is directly beneficial to the microwave dielectric properties of the samples.

Raman spectroscopy is a highly sensitive spectroscopic technique for probing the local structure of atoms. In this work, Raman spectroscopy was used to further understand how the intrinsic dielectric properties of the $Mg_{2-x}Cu_xSiO_4$ ceramics were affected by the concentration of Cu. The Raman spectra of the $Mg_{2-x}Cu_xSiO_4$ ceramics sintered at 1250 °C are presented in Fig. 6. The theoretical number of the possible optical modes of Mg_2SiO_4 that crystallises in the space group Pbnm (point group D_{2h}) can be deduced by symmetry analysis using the Bilbao Crystallographic Server [25]. Through factor group analysis, optical modes are possible based on the following irreducible representations:

Table 2
The reliability factors and fractions of the Mg_2SiO_4 and $MgSiO_3$ phases of $Mg_{2-x}Cu_xSiO_4$ from XRD refinement.

x	0	0.04	0.08	0.12	0.16	0.20	0.40
R_p (%)	9.09	10.3	10.6	11.7	12.6	13.0	14.2
R_{wp} (%)	11.9	13.7	14.0	15.7	17.0	17.5	19.0
R_{exp} (%)	10.51	10.23	10.21	10.40	10.33	10.43	10.43
χ^2	1.28	1.78	1.88	2.28	2.72	2.82	3.32
Mg_2SiO_4 (wt%)	90.06(0.22)	98.43(0.77)	98.58(0.55)	99.79(0.53)	99.57(1.46)	99.07(1.98)	95.42(2.50)
$MgSiO_3$ (wt%)	9.94(0.24)	1.57(0.14)	1.42(0.01)	0.21(0.13)	0.43(0.02)	0.93(0.16)	4.58(1.53)

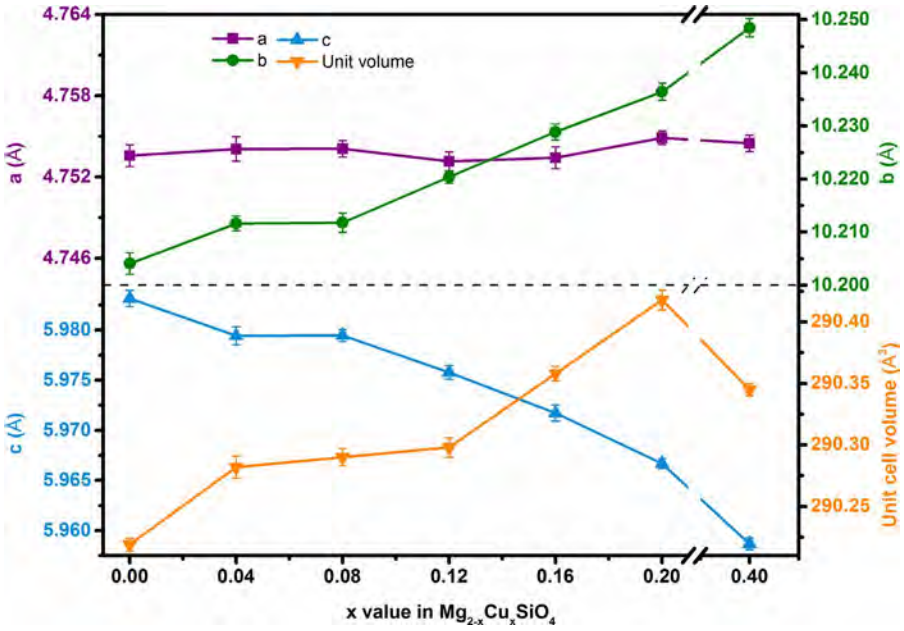

Fig. 4. The cell parameters of $Mg_{2-x}Cu_xSiO_4$ ceramics sintered at 1250 °C.

$$\Gamma_{Raman} = 11A_g + 11B_{1g} + 7B_{2g} + 7B_{3g} \quad (3)$$

Factor group analysis indicated that the Mg_2SiO_4 crystal possessed 36 vibrational modes of Raman active. In Mg_2SiO_4, the Mg(1) atoms occupy centrosymmetric sites and cannot contribute to Raman scattering. According to the previous study [26–30], the Raman mode at 148 cm^{-1} can be assigned to the SiO_4 tetrahedral translations. Mg(2) translations and SiO_4 rotations and translations were found to be located at a wide range of 192–550 cm^{-1}. The Raman modes above 500 cm^{-1} present atomic displacement dominated by motions internal to the SiO_4 tetrahedra. These internal modes are conveniently described using the conventional tetrahedral mode labels ν_1, ν_2, ν_3 and ν_4. These internal tetrahedral modes are dominated by displacements within the highly polarisable oxygen environments surrounded by covalently bonded Si and ionically bonded Mg^{2+}. The Raman modes at 450–650 cm^{-1} can be attributed to the bending vibration of SiO_4 tetrahedra. The strong modes at 800–1000 cm^{-1} can be due to the SiO_4 tetrahedral stretching. In addition, the band at 1122 cm^{-1} was present in the entire sample and attributed to the Si–O–Si vibration. As the Raman modes are very sensitive to the nature of bonding and distribution of cations at the respective Wyckoff sites, substitutions of Cu^{2+} ions for Mg^{2+} ions (Mg(1) sites) show considerable changes in the Raman spectra of these compositions [31]. Raman peak positions are sensitive to short-range order [32]. The Raman modes at 303 cm^{-1} (A_g), 590 cm^{-1} (B_{1g}) and 963 cm^{-1} (B_{3g}) shift toward lower frequency, whereas the Raman modes at 824 cm^{-1} (B_{2g}) and 920 cm^{-1} (B_{1g}) shift toward higher frequency with increasing Cu^{2+} ion content, revealing the change in short-range order for the SiO_4 tetrahedra. Changes in the cation–oxygen bond lengths and masses of the Mg(1) ions by the substitution of Cu^{2+} ions may be responsible for the short-range order and result in the shift in the Raman modes of these compositions [31]. Moreover, a new band appears at around 804 cm^{-1} at $x \geq 0.04$, and the intensity increases with the increasing Cu^{2+} ion concentration. The substitution of Cu^{2+} ions can reduce the overlapping of SiO_4 tetrahedra vibration as a result of the new band appearance.

The ε_r values of $Mg_{2-x}Cu_xSiO_4$ ceramics as a function of Cu^{2+} ion content with varying sintered temperature is revealed in Fig. 7(a). The ε_r values increase with increasing Cu^{2+} ion content at the same sintered temperature. According to Shannon [33], molecular polarisabilities of complex substances can be broken up into the ion polarisabilities. In the case of $Mg_{2-x}Cu_xSiO_4$, molecular polarisability can be estimated from the following equation:

$$\alpha(Mg_{2-x}Cu_xSiO_4) = (2-x)\alpha(Mg^{2+}) + x\alpha(Cu^{2+}) + \alpha(Si^{4+}) + 4\alpha(O^{2-}) \quad (4)$$

The ionic polarisability of Cu^{2+} (2.11 $Å^3$) is larger than that of Mg^{2+} (1.32 $Å^3$). Larger polarisability can yield larger dielectric constant. In addition, the change in ε_r values is closely related to the relative density. The higher densifications yield larger dielectric constants. Fig. 7(b) presents the relative density of $Mg_{2-x}Cu_xSiO_4$ ceramics as a function of Cu^{2+} ion content with varying sintered temperature. Evidently, the substitution of Mg^{2+} ions by Cu^{2+} ions readily reduced the sintering temperature and promoted the densification of $Mg_{2-x}Cu_xSiO_4$ ceramics. The results of relative density are consistent with the change in ε_r values.

The Qf values of the $Mg_{2-x}Cu_xSiO_4$ ceramics as a function of x are shown in Fig. 8(a). The Qf values are not only related to the intrinsic loss such as the lattice vibrational modes and ordering structure, but also to extrinsic losses, such as porosity, grain boundaries and secondary phases [12,24,34,35]. At the same sintering temperature with different Cu^{2+} ion contents, the Qf value firstly increased up to the maximum and then decreased with the substitutions of Cu^{2+} ions for Mg^{2+} ions. The Qf values related to degree of crystallization and relative density. The Raman peak intensities are more sensitive to degree of crystallization. The intensity of Raman peak increase at 856 cm^{-1}, which is assigned to $\nu_1[(SiO_4)^{4-}]$ vibration, was presented in Fig. 8(b) sintered at 1250 °C. The Raman intensities firstly decrease and then increase as $0 \leq x \leq 0.12$, while Raman intensities decrease as $0.12 < x \leq 0.40$. The relative densities, which agree with the microstructure, firstly increase and then decrease. High crystallinity and relative density was simultaneously observed as $x = 0.12$. In addition, the microstructure (porosity, grain boundary, etc) and secondary phases have influence on the Qf values. The homogeneous and dense microstructures were obtained as $0.12 \leq x \leq 0.16$ sintered at 1250 °C (Fig. 5(c) and (d)). The fraction of secondary phases showed that the minimum $MgSiO_3$ content was presented as $x = 0.12$ (Table 2). These results show that the Qf values firstly increase and reach the maximum values at $x = 0.12$, and then decrease (Fig. 8). At the different sintering temperature with the same Cu^{2+} ion contents, the microstructure depends on the sintering temperature. The optimized sintering temperature, which leads to dense microstructure, can help to decrease the extrinsic dielectric loss and enhance the Qf values [36]. The homogeneous and dense microstructure was obtained as $x = 0.08$ and 0.12 sintered at 1250 °C compare with sintered at 1200 °C, 1300 °C and

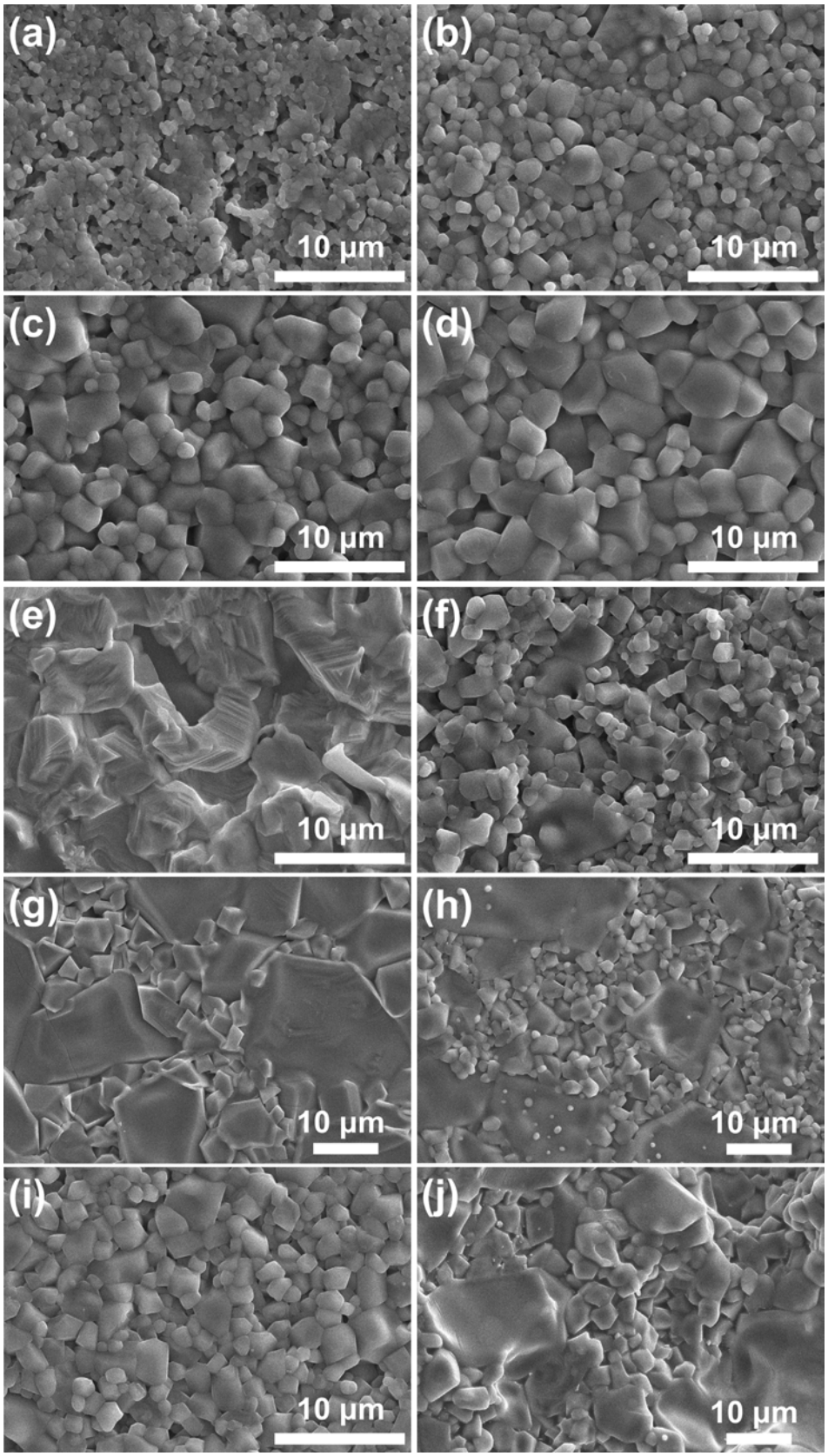

Fig. 5. SEM images of $Mg_{2-x}Cu_xSiO_4$ ceramics sintered at 1250 °C (a) $x = 0$, (b) $x = 0.08$, (c) $x = 0.12$, (d) $x = 0.16$, (e) $x = 0.40$, $x = 0.08$ sintered at (f) 1200 °C, (g) 1300 °C, (h) 1350 °C, and $x = 0.12$ sintered at (i) 1200 °C, (j) 1300 °C.

1350 °C (Fig. 5 (b, f, g and h) and Fig. 5 (c, i and j)). This result indicates that the optimum Qf values can be obtained as sintered at 1250 °C.

The τ_f values of the $Mg_{2-x}Cu_xSiO_4$ ceramics are shown in Fig. 9(a). In the figure, the τ_f firstly increases and then decreases with the substitutions of Cu^{2+} ions for Mg^{2+} ions. The τ_f values were negative because of the presence of in-phase and anti-phase tilting of the octahedral [37]. In general, τ_f was related to the temperature coefficient of the dielectric constant (τ_ε) through the following equation:

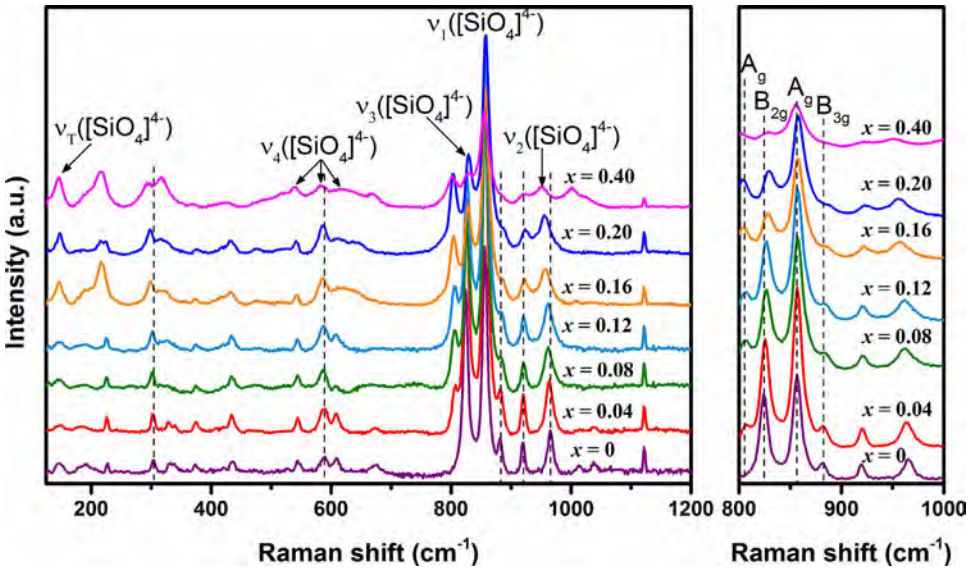

Fig. 6. Raman spectra of the $Mg_{2-x}Cu_xSiO_4$ ceramics sintered at 1250 °C.

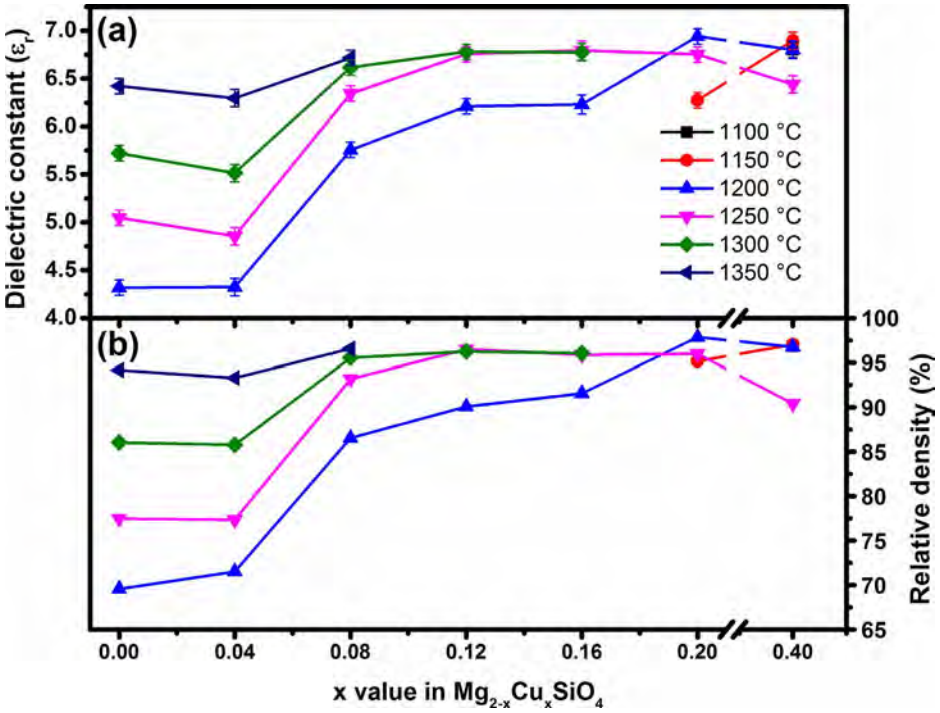

Fig. 7. The ε_r values (a) and relative density (b) of $Mg_{2-x}Cu_xSiO_4$ (x = 0–0.40) ceramics sintered at different temperatures.

$$\tau_f = -\left(\alpha + \frac{1}{2}\tau_\varepsilon\right) \approx -\left(\alpha + \frac{(\varepsilon_r - 1)(\varepsilon_r + 2)}{6\varepsilon_r \alpha_m}\left(\frac{\partial \alpha_m}{\partial T}\right)_V\right) \quad (5)$$

where α is the linear expansion coefficient and α ≈ 10 ppm/°C. Hence, τ_f mainly depends on τ_ε. Furthermore, the τ_ε depends on the structure of the compounds (such as the restoring forces acting on the ions) rather than their compositions [38]. The restoring forces were found to be positively correlated with octahedral distortions [39]. Therefore, the τ_f is directly proportional to the octahedral distortions. The correlation between τ_f values and $Mg(2)O_6$ octahedral distortion for $Mg_{2-x}Cu_xSiO_4$ (x = 0–0.40) ceramics sintered at 1250 °C are presented in Fig. 9(b). The variations in τ_f values agree with the change in the $Mg(2)O_6$ octahedral distortion, indicating that the rigid $Mg(2)O_6$ octahedral distortion is correlatesd to the τ_f values.

4. Conclusions

In the present work, $Mg_{2-x}Cu_xSiO_4$ (x = 0–0.40) ceramics were prepared using solid-state reaction method. The substitutions of Cu^{2+} ions for Mg^{2+} ions exert evident effects on the structure and microwave dielectric properties. The Cu^{2+} ions uniformly distribute across the area. The Cu^{2+} ions preferentially occupy Mg(1) site, which is confirmed by first-principle calculations and XRD refinement. In addition, partial substitution of Cu^{2+} ions for $Mg(1)^{2+}$ ions increases the cell volume, and changes the bond length and distortion of the MgO_6 octahedron of the $Mg_{2-x}Cu_xSiO_4$ phase. These structural changes on the $Mg_{2-x}Cu_xSiO_4$ affect the microwave dielectric properties. The ε_r values increase with Cu-substituted Mg. Meanwhile, The Qf values first increase and then decrease with Cu-substituted Mg, as well as increasing

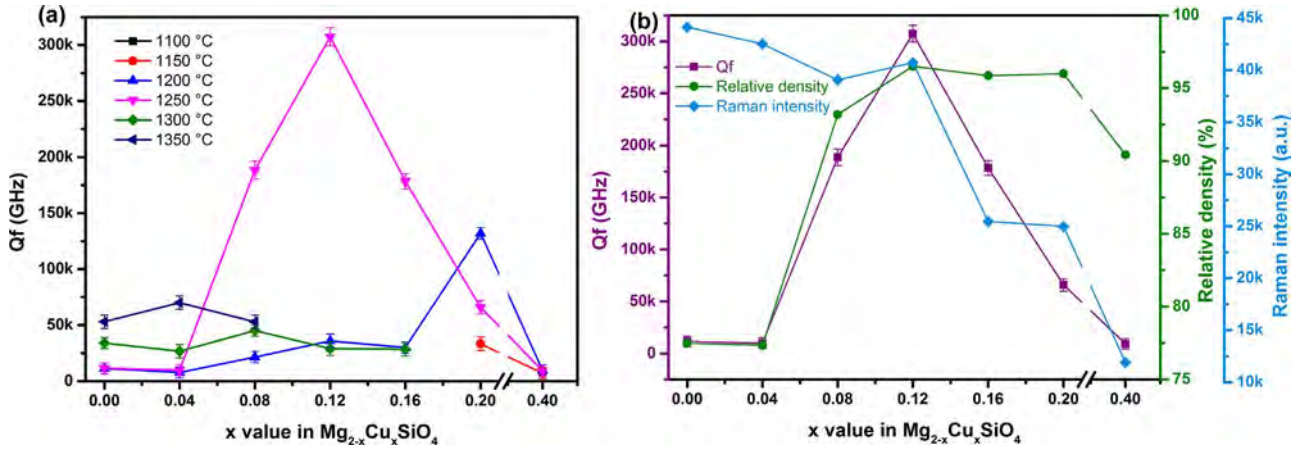

Fig. 8. The Qf values of $Mg_{2-x}Cu_xSiO_4$ (x = 0–0.40) ceramics sintered at different temperatures (a), and Qf values of the ceramics sintered at 1250 °C versus relative density and Raman intensity.

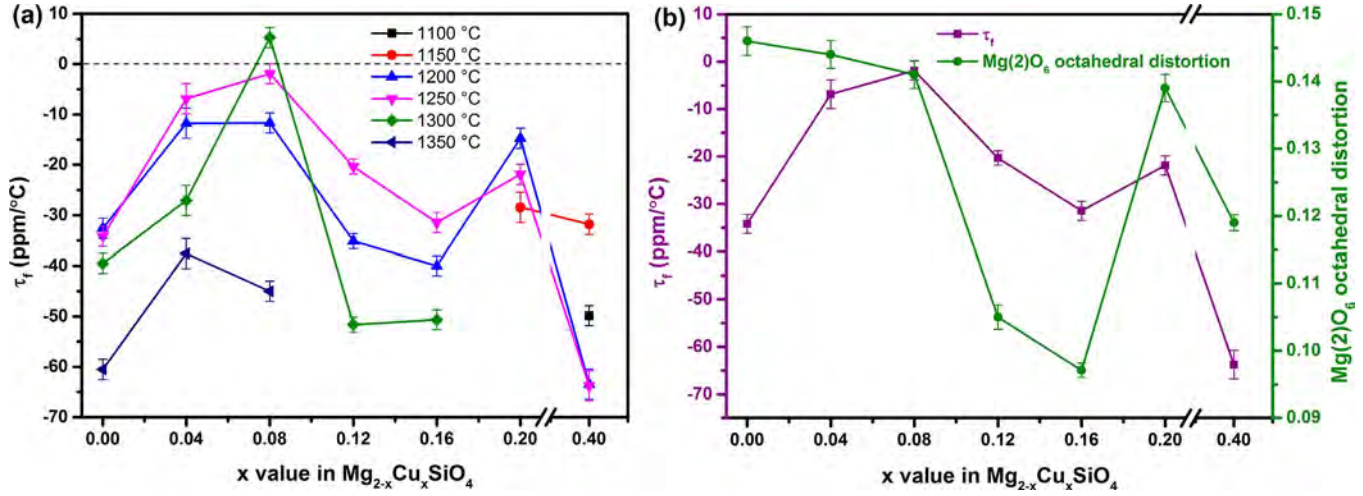

Fig. 9. The τ_f values of $Mg_{2-x}Cu_xSiO_4$ (x = 0–0.40) ceramics sintered at different temperatures (a), and τ_f values of the ceramics sintered at 1250 °C versus $Mg(2)O_6$ octahedral distortion.

sintering temperature. The distortion of MgO_6 octahedron was modified by Cu^{2+} ions, resulting in a beneficial change in τ_f values. Notably, the $Mg_{1.92}Cu_{0.08}SiO_4$ solid solution exhibits significant advantages at low sintering temperature (1250 °C), high Qf value (~188,500 GHz) and small negative τ_f values (~ −2.0 ppm/°C) compared with a pure Mg_2SiO_4 ceramic. Thus, ceramic is considered a possible candidate for millimeter-wave device applications.

Acknowledgements

This work was supported by National Natural Science Foundation of China under Grant Nos. 51372031 and 61471096, Science and Technology Department of Sichuan Province Nos. 2016JQ0016 and 2016GZ0258, National High-tech R & D Program of China under Grant No. 2015AA034102, National Key Research and Development Plan No. 2016YFA0300801.

Appendix A. Supplementary data

Supplementary data associated with this article can be found, in the online version, at http://dx.doi.org/10.1016/j.jeurceramsoc.2017.10.035.

References

[1] K.X. Song, X.M. Chen, Phase evolution and microwave dielectric characteristics of Ti-substituted Mg_2SiO_4 forsterite ceramics, Mater. Lett. 62 (2008) 520–522, http://dx.doi.org/10.1016/j.matlet.2007.05.078.
[2] I.-J. Shon, H.-S. Kang, J.-M. Doh, J.-K. Yoon, Rapid synthesis and consolidation of nanostructured Mg_2SiO_4-$MgAl_2O_4$ composites, Mater. Trans. 52 (2011) 2007–2010, http://dx.doi.org/10.2320/matertrans.M2011188.
[3] J. Sugihara, K. Kakimoto, I. Kagomiya, H. Ohsato, Microwave dielectric properties of porous Mg_2SiO_4 filling with TiO_2 prepared by a liquid phase deposition process, J. Eur. Ceram. Soc. 27 (2007) 3105–3108, http://dx.doi.org/10.1016/j.jeurceramsoc.2006.11.032.
[4] T. Tsunooka, M. Androu, Y. Higashida, H. Sugiura, H. Ohsato, Effects of TiO_2 on sinterability and dielectric properties of high-Q forsterite ceramics, J. Eur. Ceram. Soc. 23 (2003) 2573–2578, http://dx.doi.org/10.1016/S0955-2219(03)00177-8.
[5] G. Dou, D. Zhou, M. Guo, Low-temperature sintered Mg_2SiO_4–$CaTiO_3$ ceramics with near-zero temperature coefficient of resonant frequency, J. Mater. Sci. Mater. Electron. 24 (2013) 1431–1438, http://dx.doi.org/10.1007/s10854-012-0945-9.
[6] J. Ma, T. Yang, Z. Fu, P. Liu, Q. Feng, L. Zhao, Low-fired Mg_2SiO_4-based dielectric ceramics with temperature stable for LTCC applications, J. Alloys Compd. 695 (2016) 3198–3201, http://dx.doi.org/10.1016/j.jallcom.2016.11.310.
[7] T.S. Sasikala, M.N. Suma, P. Mohanan, C. Pavithran, M.T. Sebastian, Forsterite-based ceramic-glass composites for substrate applications in microwave and millimeter wave communications, J. Alloys Compd. 461 (2008) 555–559, http://dx.doi.org/10.1016/j.jallcom.2007.07.084.
[8] H. Yang, E. Li, C. Sun, S. Duan, Y. Yuan, B.I.N. Tang, The influence of sintering temperature on the microwave dielectric properties of Mg_2SiO_4 ceramics with CaO-B_2O_3-SiO_2 addition, J. Electron. Mater. 46 (2017) 1048–1054, http://dx.doi.org/10.1007/s11664-016-5046-8.
[9] T.S. Sasikala, C. Pavithran, M.T. Sebastian, Effect of lithium magnesium zinc borosilicate glass addition on densification temperature and dielectric properties of

Mg_2SiO_4 ceramics, J. Mater. Sci. Electron. 21 (2010) 141–144, http://dx.doi.org/10.1007/s10854-009-9882-7.
[10] R. Ratheesh, M. Wöhlecke, B. Berge, T. Wahlbrink, H. Haeuseler, E. Rühl, et al., Raman study of the ordering in $Sr(B'_{0.5}Nb_{0.5})O_3$ compounds, J. Appl. Phys. 88 (2000) 2813, http://dx.doi.org/10.1063/1.1287762.
[11] E.S. Kim, C.J. Jeon, J.S. Kim, S.J. Kim, Effects of crystal structure on microwave dielectric properties of ceramics, J. Korean Ceram. Soc. 45 (2008) 251–255.
[12] C. Zhang, R. Zuo, J. Zhang, Y. Wang, Structure-dependent microwave dielectric properties and middle-temperature sintering of forsterite $(Mg_{1-x}Ni_x)_2SiO_4$ ceramics, J. Am. Ceram. Soc. 98 (2015) 702–710, http://dx.doi.org/10.1111/jace.13347.
[13] T. Sugiyama, H. Ohsato, T. Tsunooka, K. Kalrimoto, Effects of ionic radii and polarizability on the microwave dielectric properties of forsterite solid solutions, Adv. Electron. Ceram. Mater. Ceram. Eng. Sci. Proc. 26 (2005) 155–160.
[14] K.X. Song, X.M. Chen, C.W. Zheng, Microwave dielectric characteristics of ceramics in Mg_2SiO_4-Zn_2SiO_4 system, Ceram. Int. 34 (2008) 917–920, http://dx.doi.org/10.1016/j.ceramint.2007.09.057.
[15] T. Sugiyama, T. Tsunooka, K. Kakimoto, H. Ohsato, Microwave dielectric properties of forsterite-based solid solutions, J. Eur. Ceram. Soc. 26 (2006) 2097–2100, http://dx.doi.org/10.1016/j.jeurceramsoc.2005.09.102.
[16] M.W. Zuo, W. Li, J.L. Shi, Q. Zeng, Influence of CuO addition to $BaSm_2Ti_4O_{12}$ microwave ceramics on sintering behavior and dielectric properties, Mater. Res. Bull. 41 (2006) 1127–1132, http://dx.doi.org/10.1016/j.materresbull.2005.11.005.
[17] C.F. Tseng, The effect CuO additive on the microwave dielectric properties of Mg $(Zr_{0.05}Ti_{0.95})O_3$ ceramics, J. Alloys Compd. 494 (2010) 252–255, http://dx.doi.org/10.1016/j.jallcom.2010.01.001.
[18] J. Rodríguez-Carvajal, Recent advances in magnetic structure determination by neutron powder diffraction, Phys. B Condens. Matter. 192 (1993) 55–69, http://dx.doi.org/10.1016/0921-4526(93)90108-I.
[19] M.D. Dyar, E.C. Sklute, O.N. Menzies, P.A. Bland, D. Lindsley, T. Glotch, et al., Spectroscopic characteristics of synthetic olivine: an integrated multi-wavelength and multi-technique approach, Am. Mineral. 94 (2009) 883–898, http://dx.doi.org/10.2138/am.2009.3115.
[20] D.L. Bish, Cation ordering in synthetic and natural Ni-Mg olivine, Am. Mineral. 66 (1981) 770–776.
[21] S. Chatterjee, S. Sengupta, T. Saha-Dasgupta, K. Chatterjee, N. Mandal, Site preference of Fe atoms in $FeMgSiO_4$ and FeMg $(SiO_3)_2$ studied by density functional calculations, Phys. Rev. B-Condens. Matter Mater. Phys. 79 (2009) 115103, http://dx.doi.org/10.1103/PhysRevB.79.115103.
[22] R.D. Shannon, Revised effective ionic radii and systematic studies of interatomie distances in halides and chaleogenides, Acta Crystallogr. Sect. A 32 (1976) 751–767.
[23] Y. Zhang, Y. Zhang, M. Xiang, Crystal structure and microwave dielectric characteristics of Zr-substituted $CoTiNb_2O_8$ ceramics, J. Eur. Ceram. Soc. 36 (2015) 1945–1951, http://dx.doi.org/10.1016/j.jeurceramsoc.2016.02.026.
[24] P. Zhang, Y. Zhao, W. Haitao, Bond ionicity, lattice energy, bond energy and microwave dielectric properties of $ZnZr(Nb_{1-x}A_x)_2O_8$ (A = Ta, Sb) ceramics, Dalt. Trans. 44 (2015) 16684–16693, http://dx.doi.org/10.1039/C5DT02164B.
[25] E. Kroumova, M.I. Aroyo, J.M. Perez-Mato, A. Kirov, C. Capillas, S. Ivantchev, et al., Bilbao crystallographic server: useful databases and tools for phase-transition studies, Phase Transitions 76 (2003) 155–170, http://dx.doi.org/10.1080/0141159031000076110.
[26] D.A. Mckeown, M.I. Bell, R. Caracas, Theoretical determination of the Raman spectra of single-crystal forsterite (Mg_2SiO_4), Am. Mineral. 95 (2010) 980–986, http://dx.doi.org/10.2138/am.2010.3423.
[27] A. Golubović, R. Gajić, M. Šćepanović, Raman and IR spectra of pure and doped forsterite single crystals, Sci. Sinter. 41 (2009) 43–47, http://dx.doi.org/10.2298/SOS0901043G.
[28] Y. Noel, M. Catti, A.R. Dovesi, The vibrational frequencies of forsterite Mg_2SiO_4: an all-electron ab initio study with the CRYSTAL code, Phys. Chem. Miner. 33 (2006) 383–393, http://dx.doi.org/10.1007/s00269-006-0085-y.
[29] E.R. Hernández, J. Brodholt, D. Alfè, Structural, vibrational and thermodynamic properties of Mg_2SiO_4 and $MgSiO_3$ minerals from first-principles simulations, Phys. Earth Planet. Inter. 240 (2015) 1–24, http://dx.doi.org/10.1016/j.pepi.2014.10.007.
[30] V.E. Shukshin, Y.K. Voronko, A.A. Sobol, Raman spectra and structure of silicon —oxygen groups in crystalline, molten, and glassy Mg_2SiO_4, AIP Conf. Proc. 1267 (2010) 1172–1173, http://dx.doi.org/10.1063/1.3482364.
[31] S.K. Singh, S.R. Kiran, V.R.K. Murthy, Structural, Raman spectroscopic and microwave dielectric studies on spinel $Li_2Zn_{(1-x)}Ni_xTi_3O_8$ compounds, Dalt. Trans. 44 (2015) 2311–2324, http://dx.doi.org/10.1039/C4DT02364A.
[32] D. Zhou, L.X. Pang, H. Wang, J. Guo, X. Yao, C.A. Randall, Phase transition, Raman spectra, infrared spectra, band gap and microwave dielectric properties of low temperature firing $(Na_{0.5x}Bi_{1-0.5x})(Mo_xV_{1-x})O_4$ solid solution ceramics with scheelite structures, J. Mater. Chem. 21 (2011) 18412–18420, http://dx.doi.org/10.1039/C1jm14004c.
[33] R.D. Shannon, Dielectric polarizabilities of ions in oxides and fluorides, J. Appl. Phys. 73 (1993) 348–366, http://dx.doi.org/10.1063/1.353856.
[34] J. Zhang, J. Zhai, X. Chou, J. Shao, X. Lu, X. Yao, Microwave and infrared dielectric response of tunable $Ba_{1-x}Sr_xTiO_3$ ceramics, Acta Mater. 57 (2009) 4491–4499, http://dx.doi.org/10.1016/j.actamat.2009.06.011.
[35] S. George, M.T. Sebastian, Synthesis and microwave dielectric properties of novel temperature stable high Q, $Li_2ATi_3O_8$ (A = Mg, Zn) ceramics, J. Am. Ceram. Soc. 93 (2010) 2164–2166, http://dx.doi.org/10.1111/j.1551-2916.2010.03703.x.
[36] D. Zhou, L. Pang, J. Guo, Z. Qi, T. Shao, Q. Wang, et al., Influence of Ce substitution for Bi in $BiVO_4$ and the impact on the phase evolution and microwave dielectric properties, Inorg. Chem. 53 (2014) 1048–1055.
[37] G.S. Babu, V. Subramanian, V.R.K. Murthy, I.-N. Lin, C.-T. Chia, H.-L. Liu, Far-infrared, Raman spectroscopy, and microwave dielectric properties of La $(Mg_{0.5}Ti_{(0.5-x)}Sn_x)O_3$ ceramics, J. Appl. Phys. 102 (2007) 64906, http://dx.doi.org/10.1063/1.2778743.
[38] C. Te Lee, C.C. Ou, Y.C. Lin, C.Y. Huang, C.Y. Su, Structure and microwave dielectric property relations in $(Ba_{1-x}Sr_x)_5Nb_4O_{15}$ system, J. Eur. Ceram. Soc. 27 (2007) 2273–2280, http://dx.doi.org/10.1016/j.jeurceramsoc.2006.07.022.
[39] S.D. Ramarao, V.R.K. Murthy, Crystal structure refinement and microwave dielectric properties of new low dielectric loss $AZrNb_2O_8$ (A: Mn, Zn, Mg and Co) ceramics, Scr. Mater. 69 (2013) 274–277, http://dx.doi.org/10.1016/j.scriptamat.2013.04.018.